HHS Public Access

Author manuscript

Neuron. Author manuscript; available in PMC 2016 July 01.

Published in final edited form as:

Neuron. 2015 July 1; 87(1): 111–123. doi:10.1016/j.neuron.2015.05.045.

Activity Regulates the Incidence of Heteronymous Sensory-Motor Connections

Alana I. Mendelsohn[1], **Christian M. Simon**[2], **L. F. Abbott**[3], **George Z. Mentis**[2], and **Thomas M. Jessell**[1]

[1]Howard Hughes Medical Institute, Kavli Institute for Brain Science, Zuckerman Mind Brain Behavior Institute, Departments of Neuroscience and Biochemistry and Molecular Biophysics, Columbia University, New York, NY 10032 USA

[2]Center for Motor Neuron Biology and Disease, Department of Pathology and Cell Biology, Columbia University, New York, NY 10032 USA

[3]Center for Theoretical Neuroscience, Departments of Physiology and Neuroscience, Columbia University, New York, NY 10032, USA

Summary

The construction of spinal sensory-motor circuits involves the selection of appropriate synaptic partners and the allocation of precise synaptic input densities. Many aspects of spinal sensory-motor selectivity appear to be preserved when peripheral sensory activation is blocked, which has led to a view that sensory-motor circuits are assembled in an activity-independent manner. Yet it remains unclear whether activity-dependent refinement has a role in the establishment of connections between sensory afferents and those motor pools that have synergistic biomechanical functions. We show here that genetically abolishing central sensory-motor neurotransmission leads to a selective enhancement in the number and density of such “heteronymous” connections, whereas other aspects of sensory-motor connectivity are preserved. Spike-timing dependent synaptic refinement represents one possible mechanism for the changes in connectivity observed after activity blockade. Our findings therefore reveal that sensory activity does have a limited and selective role in the establishment of patterned monosynaptic sensory-motor connections.

Introduction

The precision of limb movements depends on spinal sensory-motor circuits that impose coordinated patterns of muscle activation. The monosynaptic sensory-motor reflex arc represents the most intensely studied of these circuits, and its assembly adheres to a core

Correspondence: tmj1@columbia.edu.

Author Contributions

A.I.M. and T.M.J. devised the project and designed experiments. A.I.M. performed the anatomical experiments and data analysis. C.M.S. and G.Z.M. performed electrophysiological experiments and analysis. L.F.A. devised and implemented the spike-timing model with input from A.I.M. and T.M.J. A.I.M. and T.M.J. prepared the manuscript.

organizing principle in which individual limb muscles are innervated by a single pool of motor neurons. But the proprioceptive sensory afferents that relay feedback from an individual muscle connect with several motor pools, primarily those that innervate muscles with synergistic biomechanical functions (Eccles et al., 1957; Frank and Westerfield, 1983; Hongo et al., 1984). Functionally related muscles operating at individual joints exert distinct torques, implying that the coordinate sensory activation of synergistic motor pools and their recipient muscles has a role in stabilizing joint trajectories (Burkholder and Nichols, 2000). The precision and evolutionary fidelity evident in this weighted sensory-motor connectivity matrix implies selectivity in synapse formation, yet the cellular principles that confer synergist specificity remain sketchy at best.

Most studies that have explored the developmental basis of sensory-motor specificity have focused on the issue of how sensory afferents establish strong “homonymous” connections with motor neuron pools innervating the same muscle, and are able to avoid motor neurons that innervate antagonist muscles. The construction of certain of these sensory-motor connections has been shown to depend on surface recognition features, as well as the position at which motor neurons settle in the ventral spinal cord (Fukuhara et al., 2013; Pecho-Vrieseling et al., 2009; Sürmeli et al., 2011). Indeed, many aspects of the selectivity and shaping of spinal sensory-motor connections have been argued to occur without any influence of patterned sensory activity (Mears and Frank, 1997). This prevailing ‘activity-independence’ view, however, is based primarily on studies showing that sensory afferents continue to avoid antagonist motor pools when their activation is blocked through muscle paralysis or loss of muscle spindle function (Mendelson and Frank, 1991; Shneider et al., 2009; Wang et al., 2012).

The issue of how sensory afferents form “heteronymous” synaptic connections withmotor neuron pools that supply the synergist muscles involved in joint stabilization has yet to be resolved. Individual sensory afferent fibers contact both homonymous and heteronymous motor neurons (Scott and Mendell, 1976). However, the strength of heteronymous sensory-motor synaptic connections is typically weaker than that of homonymous connections, a reflection of the lower fraction of motor neurons contacted, as well as the lower density of synaptic boutons present on each motor neuron (Brown and Fyffe, 1981; Burke and Glenn, 1996; Mendell and Henneman, 1968; Nelson and Mendell, 1978; Scott and Mendell, 1976). Consequently, the formation of appropriately weighted heteronymous connections is likely to involve both the selection of appropriate synaptic partner, as well as the scaling of synaptic input strength. Intriguingly, reports of the preservation of antagonist selectivity following sensory afferent silencing by muscle paralysis also suggest the formation of novel heteronymous connections that were not observed in control animals (Mendelson and Frank, 1991). It remains possible, therefore, that sensory activity has an as yet unappreciated role in shaping heteronymous sensory-motor connections.

We set out to re-examine the issue of whether neural activity influences the specificity of sensory-motor connections, through a focus on proprioceptor connectivity with heteronymous motor neurons. To avoid uncertainties about the persistence of central transmitter release under conditions of peripheral sensory inactivity, we blocked the spontaneous and evoked release of excitatory transmitter from the central terminals of

developing proprioceptive sensory afferents through *parvalbumin* gene locus (*Pv*)- mediated expression of tetanus toxin light chain subunit (TeNT). Under conditions in which central sensory-motor transmission was virtually absent, we detected a selective increase in the number of heteronymous sensory connections with synergistic motor pools. Sensory afferents contacted a larger fraction of heteronymous motor neurons, and the density of sensory bouton contacts on each motor neuron was increased. In contrast, there was no change in the density of synaptic connections with homonymous or antagonistic motor pools. The anatomical asymmetry inherent in the monosynaptic reflex arc, together with known differences in the temporal burst patterns of synergist motor pools, led to the construction of a spike-timing dependent model of synaptic refinement that reproduces our experimental findings. We conclude that sensory afferent activity does play a role in defining one selective aspect of the fine pattern of monosynaptic sensory-motor connectivity.

Results

Defining Patterns of Heteronymous Sensory-Motor Connectivity

To examine the sensory innervation of synergist motor neurons, we focused on motor pools within the anterolateral crural (AC) synergy group that innervate muscles with defined biomechanical functions (Nichols, 1994). The tibialis anterior (TA), extensor digitorum longus (EDL), and peroneus longus (PL) muscles act synergistically to dorsiflex the ankle, but have distinct secondary biomechanical functions, with the TA adducting and the PL abducting the ankle, and the EDL extending the toes (Figures 1A and 1B; Nichols, 1994).

We explored the pattern of connectivity between these three motor pools using an activity-independent assay that exploits the transganglionic transport of cholera toxin B subunit (CTB), but not rhodamine dextran (Rh-Dex), within sensory neurons, such that after muscle injection, CTB alone accumulates in proprioceptive sensory terminals on motor neurons, which can be marked in an independent and selective manner by the presynaptic expression of vGluT1 (Betley et al., 2009; Sürmeli et al., 2011). This distinction permits a binary comparison of the density of CTB-labeled sensory terminals in contact with homonymous CTB-labeled or heteronymous Rh-Dex-labeled motor neurons (Figures S1A-S1C). We used this assay to assess the specificity of homonymous and heteronymous sensory-motor connections within the AC synergy group at postnatal days 7 and 21, monitoring both the fraction of motor neurons receiving input from sensory neurons conveying feedback from a defined muscle, as well as the density of synaptic contacts on each motor neuron.

After CTB injection into TA, EDL or PL muscles in p21 wild-type mice, we found that all CTB-labeled motor neurons received vGluT1^{+} CTB-labeled sensory contacts (Figure 1C). This finding is consistent with physiological reports that nearly all motor neurons within a pool receive homonymous sensory input (Mendell and Henneman, 1968). For each of these three motor pools, CTB was detected in ~30% of all vGluT1^{+} sensory boutons (Figure 1D). By normalizing for the efficiency of CTB labeling across motor pools, we estimate that ~70% of monosynaptic sensory inputs to motor neurons derive from homonymous sensory afferents (see Supplemental Experimental Procedures), a value consistent with connectivity in adult cat (Brown, 1981). Based on these values, we calculate that transganglionic tracing

labels ~40-50% of all homonymous contacts on any given motor neuron. The incomplete efficiency of synaptic terminal labeling likely has its basis in the limited access of tracer to all muscle spindles under conditions that restrict the spread of tracer to a single muscle. Despite the lack of complete coverage, these findings suggest that transganglionic tracing labels a representative fraction of homonymous sensory-motor contacts.

We examined the percentage of motor neurons receiving heteronymous sensory input for each of the six possible sensory-motor pairs within the AC synergy group. We found that 42% of TA motor neurons received sensory input from EDL afferents, and that 52% of EDL motor neurons received input from TA afferents (Figure 1C). These values are consistent with physiological reports that ~40-70% of motor neurons within a pool receive heteronymous sensory input from a given muscle (Nelson and Mendell, 1978; Scott and Mendell, 1976). In contrast, only 4% of TA motor neurons and 12% of EDL motor neurons, respectively, received input from PL afferents. Moreover, only 3% and 7% of PL motor neurons, respectively, received sensory input from TA and EDL afferents. Thus, the TA and EDL motor pools, but not the PL pool, are linked by prominent heteronymous feedback in their sensory-motor reflex arcs (Figure 1G). Finally, we determined that gastrocnemius (GS) motor neurons, which serve an antagonist ankle extensor function, did not receive TA sensory feedback (Figure 6A).

We next assessed the density and distribution of heteronymous synaptic contacts on each motor neuron. Input from EDL sensory afferents represented 9% of all $vGluT1^+$ boutons on TA motor neurons and similarly, 10% of all $vGluT1^+$ boutons on EDL motor neurons were labeled by TA sensory afferents (Figure 1D). Moreover, the somatic and dendritic distribution of these heteronymous boutons exhibited a proximal bias, a distribution similar to that of their homonymous counterparts (Figures S1D and S1F). We determined that the ratio of heteronymous to homonymous input was 0.29 for EDL motor neurons receiving TA sensory afferent input, and 0.38 for TA motor neurons receiving EDL sensory input (see Supplemental Experimental Procedures). Only rare PL motor neurons received sensory input from TA or EDL afferents, and these typically received only a single synaptic contact, an indication that PL lacks functional sensory feedback from TA or EDL afferents.

We next examined whether the pattern of heteronymous connections apparent at p21 is evident at earlier postnatal stages, closer to the late embryonic stages during which sensory-motor synapses first form. To address this issue, we assayed representative heteronymous connections formed by TA sensory afferents at p7. We were not able to perform these experiments at earlier stages due to the inefficiency of neonatal CTB labeling, a likely consequence of lower levels of expression of the surface ganglioside GM1, the CTB receptor (Yu, 1994). We found that the percentage of motor neurons receiving TA input at p7 was similar to that at p21: TA sensory afferents contacted all TA motor neurons, as well as 32% of EDL motor neurons, and no PL motor neurons (Figure 1E). Moreover, when we examined the density of contacts formed by TA sensory afferents, we found that CTB accumulated in 7% of $vGluT1^+$ TA sensory boutons in contact with EDL motor neurons, a bouton density comparable, if slightly lower, to that observed at p21 (Figure 1F). The lower density of synaptic labeling at p7 is most likely attributable to the decreased efficiency of CTB transport at early postnatal ages. Our findings indicate that both the target specificity

and the relative density of heteronymous sensory-motor connections are established by the first postnatal week.

Functional Validation of Heteronymous Connection Specificity and Density

We next asked whether the anatomically defined pattern of heteronymous connectivity provides an accurate reflection of the functional density of proprioceptive sensory input. To evaluate this issue, the physiological strength of proprioceptive sensory input was assessed in wild-type mice *in vitro* at p2-p6, by intracellular recording from retrogradely-labeled TA or PL motor neurons in combination with selective stimulation of individual muscles (Figure 2A). We used early postnatal preparations because at this stage, CTB-488-labled motor neurons are more easily visualized for targeted physiology (Figure 2B). In these studies, unlabeled EDL motor neurons were identified by the absence of CTB-488 accumulation following TA or PL retrograde labeling, and by the presence of large amplitude EPSPs upon EDL sensory nerve stimulation. Sensory-motor EPSPs were identified as monosynaptic on the basis of their low (<0.02) coefficient of variation in time of EPSP onset at 1 Hz stimulation frequency (Doyle and Andersen, 2001; Shneider et al, 2009). The amplitude of the monosynaptic EPSP was measured 3 ms from the onset of the response (Mears and Frank, 1997; Shneider et al., 2009). The latency of the monosynaptic EPSP following stimulation of the muscle was measured from the onset of the stimulus artifact to the onset of the response.

We found that TA motor neurons exhibited mean EPSP amplitudes of 5.5 mV after TA muscle stimulation, of 2.1 mV after EDL muscle stimulation, and negligible activation (<0.1 mV) after PL muscle stimulation (Figures 2C-2E and S2A). Similarly, EDL motor neurons generated EPSPs with mean amplitudes of 8.2 mV upon EDL sensory stimulation, of 3.5 mV upon TA stimulation and of <0.1 mV upon PL stimulation (Figures S2F-S2H). The average heteronymous to homonymous input ratio for TA motor neurons receiving EDL input was 0.43 (Figure 2F), and for EDL motor neurons receiving TA input was 0.39 (Figure S2I). PL motor neurons exhibited EPSPs of 14.8 mV upon PL stimulation, of 3.3 mV upon EDL stimulation, and of <0.1 mV for TA stimulation (Figures 2G-2I and S2B-S2D). The average ratio of heteronymous to homonymous input for PL motor neurons receiving EDL input was 0.20 (Figure S2E).

Thus, the only discrepancy between anatomical and physiological assay methods is the presence of a minor EDL sensory input to PL motor neurons, detected physiologically but not anatomically. This may reflect the underrepresentation of EDL sensory bouton labeling density, a consequence of the difficulty of achieving focal tracer injections into the small, thin EDL muscle. Overall, these physiological studies indicate that anatomical tracing of synaptic bouton density is a reliable measure of both the specificity and relative density of heteronymous sensory inputs across different motor pools.

Motor Pool Position is Unlikely to Determine Patterns of Heteronymous Connectivity

We considered whether the settling position of motor neurons might contribute to the pattern of heteronymous connectivity. This possibility was raised by studies on the formation of homonymous sensory-motor connections, where motor neuron positional order has a role in

shaping homonymous connectivity – a reflection of the fact that motor pools are clustered together within the ventral spinal cord at dorsoventral positions that match the independently assigned termination zones of their homonymous sensory afferents (Sürmeli et al., 2011). These findings prompted us to examine whether the specificity of heteronymous connections could simply be a function of a finer-grained positional segregation of motor pools, within micro-domains that represent local target zones for different sets of sensory afferents.

To resolve this issue, we mapped the settling positions of the TA, EDL and PL motor pools at rostrocaudal levels L3-L4 at p7 and p21, assigning positional coordinates to individual motor neurons within each pool with respect to the position of the central canal (Figure 3A). We observed considerable overlap in individual motor neuron cell body positions at p21, with ~90% of motor neurons in each pool located within 150 μm of the centroid of neighboring synergist pools (Figure S3A). Moreover, the dendrites of neurons within each pool overlapped with the dendrites of motor neurons from neighboring pools (Figure 3A). Nevertheless, we found that the three pool centroids were distinct, and most tellingly, were roughly equidistant from one another (Figure 3B). The same positional relationships were detected in p7 mice (Figures 3C, 3D and S3B), an expected finding since motor pool settling is apparent by embryonic day 14 (Demireva et al., 2011; De Marco Garcia and Jessell, 2008). The anatomical equidistance of these three motor pools contrasts with the marked asymmetry in heteronymous sensory synaptic density. Taken together with the degree of proximity and dendritic overlap between the three pools, we conclude that the settling of motor neurons within smaller micro-domains is an unlikely determinant of observed sensory patterns of heteronymous connectivity.

Tetanus Toxin Expression in Proprioceptors Blocks Sensory-Motor Transmission

We next turned to the potential contribution of sensory transmitter release and consequent activity in the establishment of heteronymous connections. To address this issue we set out to block central sensory-motor neurotransmission through expression of tetanus toxin light chain subunit (TeNT), a toxin that blocks neurotransmitter release through cleavage of the synaptic vesicle fusion proteins VAMP 1 and VAMP 2 (Humeau et al., 2000). A *Pv::cre* driver line, which directs transgene expression in embryonic proprioceptive sensory neurons at the time during which sensory-motor connections first form (Hippenmeyer et al., 2005), was crossed to a *ROSA26*$^{floxstop\text{-}TeNT}$ mouse strain (Zhang et al., 2008) to generate *Pv*^{TeNT} mice. These transgenic mice exhibited severe defects in motor coordination, yet survived until p18, permitting us to assess the general impact of tetanus toxin expression in sensory afferents through examination of the number and morphology of sensory-motor synapses.

Proprioceptor afferent trajectory, muscle spindle morphology and the number of Pv^{+} sensory neurons were unaltered by sensory expression of tetanus toxin (Figures 4A, S4A and S4B). Moreover, cytochemically-defined sensory-motor synapses form in *Pv*^{TeNT} mice and were detected in numbers similar to that in wild-type (*Pv::cre*$^{+/-}$) littermates (Figures 4B-4D). A small fraction (~15%) of vGluT1^{+} sensory bouton contacts with motor neurons exhibited a larger cross-sectional area in *Pv*^{TeNT} mice, in some cases up to 2.5-fold greater than the mean value in wild-type mice, implying an activity-dependent constraint on synaptic volume (Figures S4C and S4D). Nevertheless, these findings indicate that expression of tetanus

toxin does not alter the density or morphology of most proprioceptive sensory terminals that contact motor neurons.

We next assessed the impact of proprioceptor tetanus toxin expression on presynaptic vesicle release proteins in proprioceptor terminals. In control studies, we found that 84% of vGluT1$^+$ bouton contacts with motor neurons expressed VAMP 1, and of these, 44% co-expressed VAMP 2 (Figure S4G). The remaining vGluT1$^+$ boutons may express lower levels of VAMP 1 or VAMP 2, or conceivably one of the other VAMP-related proteins (Hong, 2005). Nevertheless, *Pv^{TeNT}* mice exhibited a 96% loss of VAMP 1 and VAMP 2 colocalization with vGluT1$^+$ boutons in contact with motor neurons (Figures 4E and S4H). Thus, expression of TeNT in proprioceptive sensory neurons effectively eliminates the two VAMP proteins most closely associated with presynaptic vesicle fusion and release.

Most crucially, we determined the extent to which sensory transmission is impaired by TeNT expression, performing both extracellular ventral root recordings and intracellular recordings from individual motor neurons. In p8 wild-type mice, dorsal root stimulation evoked large (2.5 mV) ventral root potentials, with the monosynaptic component defined as the potential recorded within 3 ms of response onset. Ventral root recordings from littermate *Pv^{TeNT}* mice revealed a 92% reduction in the amplitude of the monosynaptic component of the sensory-motor reflex in response to dorsal root stimulation (Figures 5A-5C). Furthermore, intracellular recordings from L4 motor neurons in p4 *Pv^{TeNT}* mice revealed a 96% reduction in the amplitude of monosynaptic EPSPs evoked by dorsal root stimulation, when compared to wild-type littermates (Figures 5D-5F). During intracellular recording, we noted that a small fraction of motor neurons in the *Pv^{TeNT}* mice were activated monosynaptically to subthreshold levels, potentially accounting for the residual amplitude observed upon extracellular recording (Figure S5). The long-latency components observed in both extracellular and intracellular motor neuron recordings are mediated by NMDA receptor activation (Mentis et al., 2005; Pinco and Lev-Tov, 1993; Ziskind-Conhaim, 1990). Thus, sensory-motor communication in *Pv^{TeNT}* mice is no longer functional.

Increased Incidence of Heteronymous Sensory-Motor Connections in *Pv^{TeNT}* Mice

The detection of sensory-motor contacts in the absence of sensory transmitter release next permitted us to examine the role of sensory-driven activity in the targeting of sensory neurons to different motor pools.

We used transganglionic CTB transport to monitor whether the loss of sensory transmitter release changes the incidence of homonymous sensory-motor connections on TA and EDL motor neurons. In *Pv^{TeNT}* mice, we determined that all CTB-labeled TA motor neurons received CTB-labeled vGluT1$^+$ sensory inputs, both at p7 and p18 (Figures 6A and 6B). Moreover, CTB accumulation in *Pv^{TeNT}* mice was detected in ~30% of vGluT1$^+$ sensory boutons on TA motor neurons, a density similar to that found in wild-type mice (Figures 6C and S6A). The incidence of EDL sensory contacts with homonymous EDL motor neurons was also unchanged in *Pv^{TeNT}* mutants (Figures S6D and S6E).

Previous studies have suggested that glutamatergic inputs to motor neurons may contribute to the establishment of mature dendritic architecture (Kalb, 1994). We therefore evaluated

the subcellular distribution of homonymous sensory bouton contacts on the cell bodies and proximal dendrites of EDL motor neurons. We found no change from the wild-type profile (Figures S6G and S6H). As in wild-type mice, TA sensory afferents in Pv^{TeNT} mice avoided forming contacts with antagonist GS or with synergist group PL motor neurons, both at p7 and p18 (Figures 6A, 6B and S6C). Taken together, these findings show that the absence of sensory-driven activity does not erode the ability of proprioceptive afferents to form homonymous synaptic connections in a selective manner, nor to avoid antagonist motor pools.

We next turned to the issue of whether sensory transmission is required for establishing the specificity or incidence of heteronymous sensory connections with synergist motor neurons. As in wild-type mice, we found in Pv^{TeNT} mutants that TA sensory afferents contacted EDL motor neurons, and conversely that EDL sensory afferents contacted TA motor neurons (Figures 6A, 6B and S6D). But at both p7 and p21, the incidence of heteronymous connections in Pv^{TeNT} mutants differed from wild-type. At both ages, the proportion of EDL motor neurons receiving TA sensory input was ~2-fold greater than in wild-type (Figures 6A and 6B). In addition, the fraction of TA motor neurons receiving EDL sensory input was ~1.6-fold greater at p18 (Figure S6D). Thus, silenced sensory afferents contact the appropriate synergist motor pools, but connect with a greater proportion of motor neurons within each pool.

We next assessed the density and distribution of heteronymous contacts on individual motor neurons in the absence of sensory-motor transmission, focusing on the density of TA-derived vGluT1$^+$ sensory bouton contacts with EDL motor neurons. At p7, individual EDL motor neurons in Pv^{TeNT} mice exhibited a ~2-fold increase in TA sensory input, compared to wild-type values (Figure 6D). By p18 this increase had partly diminished, such that EDL neurons now received a ~1.4-fold increase in TA sensory input compared to wild-type values (Figure S6B). Heteronymous sensory boutons had similar cross-sectional areas to homonymous boutons in Pv^{TeNT} mice, as in wild-type mice (Figures S1I and S4F). Moreover, there was no detectable change in the subcellular distribution of heteronymous sensory boutons in Pv^{TeNT} mice, when compared with wild-type controls (Figures S6I and S6J). Thus in the absence of sensory transmission, motor neurons receive supernumerary heteronymous sensory inputs. The relative density of synaptic inputs decays gradually, however, over the first three postnatal weeks.

Discussion

The coordinate activation of motor synergy groups by proprioceptive sensory afferents is thought to promote the stabilization of limb trajectories, yet the strategies involved in establishing heteronymous sensory connections with synergist motor pools have not been resolved. Our genetic studies in mice show that proprioceptive afferents form incorrectly tuned heteronymous sensory-motor connections in the absence of central sensory transmission, whereas the specificity and incidence of homonymous and antagonist connectivity is unchanged. Taken together, our observations establish that activity-dependent mechanisms do have a role in determining appropriate patterns of sensory-motor connectivity.

Sensory Afferent Activity and the Refinement of Synaptic Density

Studies to define the origins of sensory-motor connectivity patterns have emphasized the activity-independence of this developmental process (Mears and Frank, 1997; Mendelson and Frank, 1991). Our findings show that the state of central sensory transmission regulates one select feature of sensory-motor connectivity - the density of heteronymous connections between sensory afferents and synergist motor neurons.

The most likely reason for these divergent conclusions is that prior studies focused on the sensory avoidance of antagonist motor pools, a finding which our data corroborate (Mears and Frank, 1997; Mendelson and Frank, 1991; Shneider et al., 2009; Wang et al., 2012). An additional difference between our findings and prior physiological studies in chick is that the chick studies demonstrated a general ~2-fold increase in the amplitude of sensory-motor EPSPs under conditions of muscle paralysis (Mendelson and Frank, 1991), whereas we observe no change in the numerical incidence, and thus the implied strength, of homonymous connections. This discrepancy could reflect differences in the strategy for sensory inactivation, since peripheral muscle paralysis reduces the programmed death of motor neurons, and potentially of proprioceptive sensory neurons (Oppenheim, 1989).

The finding that the state of sensory transmitter release sets the synaptic density of a defined class of sensory-motor connections brings proprioceptive sensory neurons into the general fold of activity-dependent circuit refinement that operates elsewhere in the central nervous system (CNS) (Okawa et al., 2014). In other circuits for instance, presynaptic activity drives the competitive elimination of motor synapses from multiply innervated muscle fibers and the elimination of supernumerary climbing fibers from cerebellar Purkinje neurons (Buffelli et al., 2003; Lorenzetto et al., 2009). Yet one aspect of the logic of synaptic pruning in the sensory-motor system differs from that of most other regions of the CNS. The set of potential postsynaptic motor neuron partners that serve as substrates for pruning can be independently identified by their molecular identity and connectivity. In nearly all other regions of the CNS, target neurons are perceived as molecularly and functionally equivalent at the time of activity-driven pruning (Okawa et al., 2014). As a consequence, analysis of the sensory-motor system permits a separation of the contribution of sensory activity to the formation of selective sensory connections with distinct motor targets and the subsequent refinement of connection densities.

One of the few other neural systems in which the refinement of connections to distinct neuronal subtypes has been explored is the mammalian retina. In the retina, dark rearing reduces sensory input activity, which impairs the maturation of connections between cone cells and particular cone-selective bipolar cell subtypes (Dunn et al., 2013). The selective consequences of this perturbation may reflect the timing of synapse formation, since connections with type 6 bipolar cells, which are established prior to eye opening, are unaffected by the loss of presynaptic activity, whereas connections with type 7 and type 8 bipolar cells, which form after activity impairment, are disrupted. One distinction between spinal cord and retina is that the loss of sensory input in the retina perturbs the formation of connections as well their subsequent elimination.

The increase in heteronymous connections observed under activity blockade could result either from synaptic sprouting or from a loss of synaptic refinement. However, the establishment of spinal sensory-motor connections does not appear to be affected by the loss of sensory transmitter release. Even though heteronymous connections double in frequency under conditions of activity-blockade, they represent only a minority of sensory inputs to motor neurons, and the overall number of sensory-motor connections remains relatively constant. Consequently, if the enrichment in heteronyomous sensory-motor connections upon sensory transmission blockade was the result of synaptic sprouting, this sprouting would have to exhibit absolute selectivity for synergist pools. Although we can not rule out the possibility that more heteronymous connections form upon sensory transmission blockade, a likelier explanation for the observed increase in heteronymous connections is a failure in the pruning of connections.

The enhanced density of heteronymous sensory-motor connections observed in these studies was achieved through central blockade of transmitter release from all proprioceptive sensory afferents. In other neural systems, synaptic remodeling typically occurs under conditions of selective input blockade, such that active synapses effectively outcompete their less active neighbors (Buffelli et al., 2002; Stellwagen and Shatz, 2002; Yu et al., 2004). It has not yet been possible to silence a single muscle-defined set of sensory afferents, but precedent in other circuits might argue that such an imbalance promotes synaptic competition and leads to the elimination of inactive synapses.

Sensory-Motor Spike Timing May Explain Synaptic Refinement

It remains unclear how heteronymous connectivity is enhanced in a selective manner. Spike-timing modes of synapse refinement offer a quantitative explanation of the way in which connections can be eliminated under conditions in which all sensory afferents exhibit equivalent levels of activity. Spike-timing rules have been invoked in developmental refinement in a few cases only, typically in cortical circuits that feature fast temporal spike correlations (<20 ms) (Butts and Kanold, 2010).

Nevertheless, spike-timing may be relevant to the spinal sensory-motor system, where motor neurons belonging to different synergist pools exhibit distinctions in their peak firing phase (Bekoff et al., 1975; Krouchev et al., 2006; Yakovenko et al., 2002). As a consequence, the relative timing of sensory input to homonymous and heteronymous motor pool targets would be expected to differ with respect to the timing of motor neuron burst activity. We therefore considered whether these experimental observations can be accounted for by a differential spike-timing model that captures the distinct temporal features of convergent homonymous and heteronymous sensory inputs onto an individual postsynaptic motor neuron (Figure 7A; Abbott and Nelson, 2000; Feldman, 2012). In the adult, extrafusal (α) motor neuron spike trains are known to be accompanied by a co-activation of the fusiform (γ) motor system, which innervates intrafusal muscle fibers and serves to sensitize sensory responses to the contraction of muscle (Hulliger et al., 1989; Hunt, 1951). During α-γ co-activation, α-motor neuron spiking drives muscle activity, and in turn, sensory firing rate (Prochazka and Gorassini, 1998). α-γ coactivation also appears to occur at early postnatal stages through the activity of beta motor axons, which innervate both extra- and intrafusal

muscle fibers (Banks, 1994). Thus for a given muscle, sensory firing rate is informed by that of the motor neuron.

We constructed a model motor neuron driven by a 2 Hz oscillating sinusoidal current designed to simulate the impact of non-sensory excitatory synaptic inputs. In this model, the motor neuron fires a burst of ~6 action potentials every 500 ms (Figure 7C), a similar pattern to that observed *in vivo* (Hoffer et al., 1987; Rossignol, 1996). We modeled two sensory populations, one homonymous and the other heteronymous. Since sensory afferents innervate distinct muscle fibers, spikes for each homonymous sensory afferent were generated by a Poisson process with a rate oscillating at the motor oscillation frequency but phase shifted relative to the motor oscillation by an amount chosen on each cycle from a zero-mean Gaussian distribution with a standard deviation of 10 degrees (Figure 7D). Because synergist muscles have distinct temporal activity patterns (Krouchev et al., 2006), heteronymous sensory afferent spikes were generated in a similar manner, except that their phase shifts were drawn from a Gaussian distribution with a larger standard deviation, of 15 degrees (Figure 7D).

The strengths of these sensory-motor synapses were modified by a standard spike-timing dependent plasticity (STDP) model in which each pair of pre- and postsynaptic action potentials changed the synaptic strength by an amount determined by their time difference (Figure 7B; Feldman, 2000; Song et al., 2000). We imposed the condition that sensory-motor synapses are subject to pruning when presynaptic sensory spikes exhibit poor temporal correlation with the motor neuron postsynaptic spike, such that any synapse with a strength <1% of the maximal synaptic conductance was eliminated. The application of this spike-timing model for a prolonged period of time would lead to the eventual elimination of an excessive number of contacts. We therefore presumed that refinement occurs only during a critical period of synaptic plasticity.

With an equal number of initial inputs of each sensory type, application of the spike-timing model for ~200-300 minutes of simulated muscle contraction led to the elimination of ~4 times as many heteronymous as homonymous synapses, resulting in a 3-to-1 final ratio of homonymous to heteronymous sensory inputs (Figures 7E and 7F). Broadening the sensory phase distribution of the heteronymous population generated a similar degree of heteronymous elimination, but with a reduced amount of homonymous refinement and over a shorter simulation period. Thus, regardless of the precise parameters used, this model supports the view that differences in the relative timing of sensory and motor activity are sufficient to drive selective refinement of heteronymous sensory-motor connections. Blockade of sensory transmission would then be expected to prevent this refinement process by precluding STDP, providing a plausible explanation for the selective increase in heteronymous connection density.

Limitations of Sensory Blockade in Shaping Patterns of Sensory-Motor Connectivity

Even under conditions in which sensory transmission is blocked, our findings show that the density of heteronymous connections to a motor pool remains lower than that from its homonymous inputs. If the state of sensory transmitter release was the sole determinant of heteronymous synaptic density, then blockade of sensory transmission might have been

predicted to equalize homonymous and heteronymous input strengths. There are several potential reasons for the persistence of distinctions in homonymous and heteronymous sensory input strength under conditions of sensory input blockade.

First, the effectiveness of our sensory inactivation strategy depends on the onset of *parvalbumin*-mediated TeNT expression. *Parvalbumin* expression by proprioceptors begins at ~e14.5, just prior to the formation of sensory-motor synapses, but may take several days to spread to all proprioceptors (Arber et al., 2000; Hippenmeyer et al., 2005; J. de Nooij, personal communication). Consequently, synaptic refinement may have proceeded during the early stages of sensory-motor synapse formation. Second, our sensory inactivation strategy preserves inputs from the many descending pathways and local interneuron circuits that do not express *parvalbumin*, and these could have an accessory role in defining sensory input strengths. Furthermore, the cortical and spinal inhibitory interneurons that do express *parvalbumin* only commence expression after the first postnatal week, and would thus be inactivated after the initial pattern of sensory-motor connections is established (Benito-Gonzalez and Alvarez, 2012; Del Rio et al., 1994).

Activity-independent mechanisms may also contribute to the initial discrimination of sensory inputs to synergist motor neurons. Motor neuron positional cues have previously been shown to constrain the motor targeting of proprioceptive sensory afferents, and consequently they could perhaps help sensory afferents discriminate between neighboring synergist motor pools (Sürmeli et al., 2011). Nevertheless, for the AC synergy group we find that synergist pools lie equidistant from each other, making it hard in this case to implicate positional cues as the basis of the markedly divergent degrees of heteronymous input.

An alternative activity-independent mechanism involves sensory recognition of motor pool surface markers. Surface recognition has been implicated in sensory discrimination between certain motor pools. One mechanism underlying sensory-motor connection specificity involves a motor neuron repellent ligand, sema3E, and its cognate sensory receptor, PlexinD1. Genetic studies in mice have shown that the engagement of this recognition system precludes synaptic connectivity between surface-matched sensory and motor neurons (Fukuhara et al., 2013; Pecho-Vrieseling et al., 2009). But regardless of molecular strategy, our findings reveal that sensory afferent activity serves as one determinant of finely tuned sensory-motor connections.

Experimental Procedures

Mouse Strains

Pv::cre (Hippenmeyer et al., 2005) and *R26*$^{floxstop\text{-}TeNT}$ (Zhang et al., 2008) have been described. All experiments were performed in accordance with the National Institutes of Health Guidelines on the Care and Use of Animals and approved by the Columbia University animal care and use committee.

Immunohistochemistry

Immunohistochemical labeling was performed on cryostat (12 μm) or vibratome (70 μm) sections as described (Sürmeli et al., 2011). Images were acquired on Zeiss LSM-510 Meta

confocal microscopes. Antibodies used in this study were as follows: goat anti-CTB (List Biological Laboratories), rabbit anti-tetramethylrhodamine (Invitrogen), goat anti-ChAT (Chemicon), rabbit anti-ChAT (Demireva et al., 2011), rabbit anti-VAMP 1 (Synaptic Systems), mouse anti-VAMP 2 (Synaptic Systems), Rabbit anti-VAMP 3 (Synaptic Systems), guinea pig anti-vGluT1 (Betley et al., 2009), and chicken anti-Pv (de Nooij et al., 2013).

Motor and Sensory Neuron Labeling

Motor neurons were retrogradely labeled *in vivo* as described (Sürmeli et al., 2011). Motor pool coordinates were assigned using IMARIS with respect to the central canal and normalized to standard spinal cord dimensions (See Supplemental Experimental Procedures). Contour distributions were calculated and plotted in MATLAB.

Quantification of Sensory Synaptic Contacts with Motor Neurons

Quantification of vGluT1$^+$ sensory bouton contacts with motor neuron somata and ~100 μm dendritic arbor was performed using 0.6 μm confocal z scans of 70 μm thick sections. γ-motor neurons were excluded from analysis based on their small size and bipolar morphology (Friese et al., 2009). Motor neuron surface area was calculated using IMARIS surface function. Bouton distance from motor neuron soma was calculated using IMARIS. Bouton cross section area was calculated using ImageJ. Average fluorescence intensity was calculated using histogram function of Adobe Photoshop.

In vitro Electrophysiology

Methods for recording from isolated spinal cord preparations have been described (Mentis et al., 2005; Shneider et al., 2009). Further details provided in Supplemental Experimental Procedures.

Spike-Timing Dependent Refinement Model

The motor neuron was modeled as an integrate-and-fire neuron with a membrane time constant of 20 ms, resting and reset potentials of −60 mV, and a threshold of −54 mV. The neuron had a membrane resistance of 10 MΩ, although this number only serves to normalize the currents and conductances of the model. The model neuron received an input current $B[\cos(2\pi t/T)]_+$, with B = 0.8 nA, T = 500 ms and the bracket indicating rectification. Each sensory action potential caused the synaptic conductance to increase instantaneously by an amount g, and then to decay exponentially with a time constant of 5 ms. The synaptic conductance g is constrained to lie between zero and a maximum value g_{max} = 1 nS. It is initialized at its maximum value. The synaptic conductance g is subject to STDP through the following procedure. Every pre-post spike pair at a synapse changes g by an amount that depends on the time difference between them. When a presynaptic spike precedes a postsynaptic spike by a time Δt, g is increased by an amount $A_+\exp(-\Delta t/\tau_+)g_{max}$ with A_+ = 0.01 and τ_+ = 10 ms. When a presynaptic spike follows a postsynaptic spike by a time Δt, g is decreased by an amount $A_-\exp(-\Delta t\tau_-)g_{max}$ with A_- = 0.00175 and τ_- = 100 ms. All spike pairs contribute in this way and their total impact is computed by summing the contributions

from each pair. If the conductance of any synapses falls below $g = 0.01 g_{max}$ the synapse is permanently eliminated.

Supplementary Material

Refer to Web version on PubMed Central for supplementary material.

Acknowledgements

We thank Martyn Goulding (Salk Institute) for generously providing the $R26^{floxstop\text{-}TeNT}$ mice; Min Dong (Harvard University) for information on VAMP expression; Richard Nichols (Georgia Tech) for insightful discussions of biomechanics; Timothy Machado for help with generating contour plots and Nicole Machac and David Wu for technical assistance. We are grateful to Richard Nichols (Georgia Tech), Rob Brownstone (Dalhousie University), Joriene de Nooij, Nikolaos Balaskas and David Ng for comments on the manuscript. We also thank an anonymous reviewer for pointing out the hazards inherent in the use of the word 'epicenter.' G.Z.M. was supported by the NIH (RO1-NS078375 and R21-NS079981) and the Department of Defense (GR.10235006). T.M.J. was supported by NIH grant NS080932, The Harold and Leila Y. Mathers Foundation and Project A.L.S, and is an HHMI investigator.

References

Abbott LF, Nelson SB. Synaptic plasticity: taming the beast. Nat. Neurosci. 2000; 3 Suppl:1178–1183. [PubMed: 11127835]

Arber S, Ladle DR, Lin JH, Frank E, Jessell TM. ETS gene Er81 controls the formation of functional connections between group Ia sensory afferents and motor neurons. Cell. 2000; 101:485–498. [PubMed: 10850491]

Banks RW. The motor innervation of mammalian muscle spindles. Prog. Neurobiol. 1994; 43:323–362. [PubMed: 7816930]

Bekoff A, Stein PSG, Hamburger V. Coordinated Motor Output in the Hindlimb of the 7-Day Chick Embryo. Proc. Natl. Acad. Sci. U. S. A. 1975; 72:1245–1248. [PubMed: 1055400]

Benito-Gonzalez A, Alvarez FJ. Renshaw Cells and Ia Inhibitory Interneurons Are Generated at Different Times from p1 Progenitors and Differentiate Shortly after Exiting the Cell Cycle. J. Neurosci. 2012; 32:1156–1170. [PubMed: 22279202]

Betley JN, Wright CVE, Kawaguchi Y, Erdélyi F, Szabó G, Jessell TM, Kaltschmidt JA. Stringent specificity in the construction of a GABAergic presynaptic inhibitory circuit. Cell. 2009; 139:161–174. [PubMed: 19804761]

Brown, AG. Organization in the Spinal Cord. Springer Verlag; New York: 1981. p. 238

Brown A, Fyffe R. Direct observations on the contacts made between Ia afferent fibres and alpha-motoneurones in the cat's lumbosacral spinal cord. J. Physiol. 1981; 313:121–140. [PubMed: 7277213]

Buffelli M, Busetto G, Cangiano L, Cangiano A. Perinatal switch from synchronous to asynchronous activity of motoneurons: link with synapse elimination. Proc. Natl. Acad. Sci. U. S. A. 2002; 99:13200–13205. [PubMed: 12242340]

Buffelli M, Burgess R, Feng G, Lobe C, Lichtman J, Sanes J. Genetic evidence that relative synaptic efficacy biases the outcome of synaptic competition. Nature. 2003; 424

Burke RE, Glenn LL. Horseradish peroxidase study of the spatial and electrotonic distribution of group Ia synapses on type-identified ankle extensor motoneurons in the cat. J. Comp. Neurol. 1996; 372:465–485. [PubMed: 8873872]

Burkholder T, Nichols T. The mechanical action of proprioceptive length feedback in a model of the cat hindlimb. Motor Control. 2000; 4:201–220. [PubMed: 11508248]

Butts DA, Kanold PO. The applicability of spike time dependent plasticity to development. Front. Synaptic Neurosci. 2010; 2:30. [PubMed: 21423516]

Delaurier A, Burton N, Bennett M, Baldock R, Davidson D, Mohun TJ, Logan MP. The Mouse Limb Anatomy Atlas: an interactive 3D tool for studying embryonic limb patterning. BMC Dev. Biol. 2008; 8:83. [PubMed: 18793391]

Demireva EY, Shapiro LS, Jessell TM, Zampieri N. Motor neuron position and topographic order imposed by β- and γ-catenin activities. Cell. 2011; 147:641–652. [PubMed: 22036570]

Dunn FA, Della Santina L, Parker ED, Wong ROL. Sensory experience shapes the development of the visual system's first synapse. Neuron. 2013; 80:1159–1166. [PubMed: 24314727]

Eccles J, Eccles R, Lundberg A. The convergence of monosynaptic excitatory afferents on to many different species of alpha motoneurones. J. Physiol. 1957; 137:22–50. [PubMed: 13439582]

Feldman D. Timing-Based LTP and LTD at Vertical Inputs to Layer II/III Pyramidal Cells in Rat Barrel Cortex. Neuron. 2000; 27:45–56. [PubMed: 10939330]

Feldman DE. The spike-timing dependence of plasticity. Neuron. 2012; 75:556–571. [PubMed: 22920249]

Frank E, Westerfield M. Development of sensory-motor synapses in the spinal cord of the frog. J. Physiol. 1983; 343:593–610. [PubMed: 6315924]

Friese A, Kaltschmidt JA, Ladle DR, Sigrist M, Jessell TM, Arber S. Gamma and alpha motor neurons distinguished by expression of transcription factor Err3. Proc. Natl. Acad. Sci. U. S. A. 2009; 106:13588–13593. [PubMed: 19651609]

Fukuhara K, Imai F, Ladle DR, Katayama K, Leslie JR, Arber S, Jessell TM, Yoshida Y. Specificity of monosynaptic sensory-motor connections imposed by repellent Sema3E-PlexinD1 signaling. Cell Rep. 2013; 5:748–758. [PubMed: 24210822]

Hippenmeyer S, Vrieseling E, Sigrist M, Portmann T, Laengle C, Ladle DR, Arber S. A developmental switch in the response of DRG neurons to ETS transcription factor signaling. PLoS Biol. 2005; 3:e159. [PubMed: 15836427]

Hoffer J, Sugano N, Loeb G, Marks W, O'Donovan M, Pratt C. Cat hindlimb motoneurons during locomotion. II. Normal activity patterns. J. Neurophysiol. 1987; 57:530–553. [PubMed: 3559691]

Hong W. SNAREs and traffic. Biochim. Biophys. Acta. 2005; 1744:120–144. [PubMed: 15893389]

Hongo T, Lundberg A, Phillips CG, Thompson RF. The Pattern of Monosynaptic Ia-Connections to Hindlimb Motor Nuclei in the Baboon: A Comparison with the Cat. Proc. R. Soc. B Biol. Sci. 1984; 221:261–289. [PubMed: 6146138]

Hulliger M, Dürmüller N, Prochazka A, Trend P. Flexible fusimotor control of muscle spindle feedback during a variety of natural movements. Prog. Brain Res. 1989; 80:87–101. discussion 57–60. [PubMed: 2634288]

Humeau Y, Doussau F, Grant NJ, Poulain B. How botulinum and tetanus neurotoxins block neurotransmitter release. Biochimie. 2000; 82:427–446. [PubMed: 10865130]

Hunt CC. The reflex activity of mammalian small-nerve fibres. J. Physiol. 1951; 115:456–469. [PubMed: 14898522]

Kalb RG. Regulation of motor neuron dendrite growth by NMDA receptor activation. Development. 1994; 120:3063–3071. [PubMed: 7720552]

Krouchev N, Kalaska JF, Drew T. Sequential activation of muscle synergies during locomotion in the intact cat as revealed by cluster analysis and direct decomposition. J. Neurophysiol. 2006; 96:1991–2010. [PubMed: 16823029]

Li Y, Burke RE. Developmental changes in short-term synaptic depression in the neonatal mouse spinal cord. J. Neurophysiol. 2002; 88:3218–3231. [PubMed: 12466442]

Lorenzetto E, Caselli L, Feng G, Yuan W, Nerbonne JM, Sanes JR, Buffelli M. Genetic perturbation of postsynaptic activity regulates synapse elimination in developing cerebellum. Proc. Natl. Acad. Sci. U. S. A. 2009; 106:16475–16480. [PubMed: 19805323]

De Marco Garcia NV, Jessell TM. Early motor neuron pool identity and muscle nerve trajectory defined by postmitotic restrictions in Nkx6.1 activity. Neuron. 2008; 57:217–231. [PubMed: 18215620]

Mears SC, Frank E. Formation of specific monosynaptic connections between muscle spindle afferents and motoneurons in the mouse. J. Neurosci. 1997; 17:3128–3135. [PubMed: 9096147]

Mendell LM, Henneman E. Terminals of single Ia fibers: distribution within a pool of 300 homonymous motor neurons. Science. 1968; 160:96–98. [PubMed: 4296007]

Mendelson B, Frank E. Specific monosynaptic sensory-motor connections form in the absence of patterned neural activity and motoneuronal cell death. J. Neurosci. 1991; 11:1390–1403. [PubMed: 2027053]

Mentis G, Alvarez F, Bonnot A, Richards D, Gonzalez-Forero D, Zerda R, O'Donovan MJ. Noncholinergic excitatory actions of motoneurons in the neonatal mammalian spinal cord. Proc. Natl. Acad. Sci. U. S. A. 2005; 102:7344–7349. [PubMed: 15883359]

Nelson SG, Mendell LM. Projection of single knee flexor Ia fibers to homonymous and heteronymous motoneurons. J. Neurophysiol. 1978; 41:778–787. [PubMed: 149185]

Nichols T. A biomechanical perspective on spinal mechanisms of coordinated muscular action: an architecture principle. Acta Anat. (Basel). 1994; 151:1–13. [PubMed: 7879588]

De Nooij JC, Doobar S, Jessell TM. Etv1 inactivation reveals proprioceptor subclasses that reflect the level of NT3 expression in muscle targets. Neuron. 2013; 77:1055–1068. [PubMed: 23522042]

Okawa H, Hoon M, Yoshimatsu T, Della Santina L, Wong ROL. Illuminating the Multifaceted Roles of Neurotransmission in Shaping Neuronal Circuitry. Neuron. 2014; 83:1303–1318. [PubMed: 25233313]

Oppenheim RW. The neurotrophic theory and naturally occurring motoneuron death. Trends Neurosci. 1989; 12:252–255. [PubMed: 2475935]

Pecho-Vrieseling E, Sigrist M, Yoshida Y, Jessell TM, Arber S. Specificity of sensory-motor connections encoded by Sema3e-Plxnd1 recognition. Nature. 2009; 459:842–846. [PubMed: 19421194]

Pinco M, Lev-Tov A. Synaptic excitation of alpha-motoneurons by dorsal root afferents in the neonatal rat spinal cord. J. Neurophysiol. 1993; 70:406–417. [PubMed: 8103090]

Prochazka A, Gorassini M. Ensemble firing of muscle afferents recorded during normal locomotion in cats. J. Physiol. 1998; 507:293–304. [PubMed: 9490855]

Del Rio JA, De Lecea L, Ferrer I, Soriano E. The development of parvalbumin-immunoreactivity in the neocortex of the mouse. Dev. Brain Res. 1994; 81:247–259. [PubMed: 7813046]

Rossignol S. Neural control of stereotypic limb movements. In Handbook of Physiology. 1996:173–216.

Scott JG, Mendell LM. Individual EPSPs produced by single triceps surae Ia afferent fibers in homonymous and heteronymous motoneurons. J. Neurophysiol. 1976; 39:679–692. [PubMed: 184256]

Shneider NA, Mentis GZ, Schustak J, O'Donovan MJ. Functionally reduced sensorimotor connections form with normal specificity despite abnormal muscle spindle development: the role of spindle-derived neurotrophin 3. J. Neurosci. 2009; 29:4719–4735. [PubMed: 19369542]

Song S, Miller KD, Abbott LF. Competitive Hebbian learning through spike-timing-dependent synaptic plasticity. Nat. Neurosci. 2000; 3:919–926. [PubMed: 10966623]

Stellwagen D, Shatz CJ. An instructive role for retinal waves in the development of retinogeniculate connectivity. Neuron. 2002; 33:357–367. [PubMed: 11832224]

Sürmeli G, Akay T, Ippolito GC, Tucker PW, Jessell TM. Patterns of spinal sensory-motor connectivity prescribed by a dorsoventral positional template. Cell. 2011; 147:653–665. [PubMed: 22036571]

Wang Z, Li L, Frank E. The role of muscle spindles in the development of the monosynaptic stretch reflex. J. Neurophysiol. 2012; 108:83–90. [PubMed: 22490553]

Yakovenko S, Mushahwar V, VanderHorst V, Holstege G, Prochazka A. Spatiotemporal activation of lumbosacral motoneurons in the locomotor step cycle. J. …. 2002; 87:1542–1553.

Yu RK. Development regulation of ganglioside metabolism. Prog. Brain Res. 1994; 101:31–44. [PubMed: 8029460]

Yu C, Power J, Barnea G, O'Donnell S, Brown H, Osborne J, Axel R, Gogos J. Spontaneous neural activity is required for the establishment and maintenance of the olfactory sensory map. Neuron. 2004; 42:553–566. [PubMed: 15157418]

Zhang Y, Narayan S, Geiman E, Lanuza GM, Velasquez T, Shanks B, Akay T, Dyck J, Pearson K, Gosgnach S, et al. V3 spinal neurons establish a robust and balanced locomotor rhythm during walking. Neuron. 2008; 60:84–96. [PubMed: 18940590]

Ziskind-Conhaim L. NMDA Receptors Mediate Poly- and Monosynaptic Potentials in Motoneurons of Rat Embryos. J. Neurosci. 1990; 10:125–135. [PubMed: 1967635]

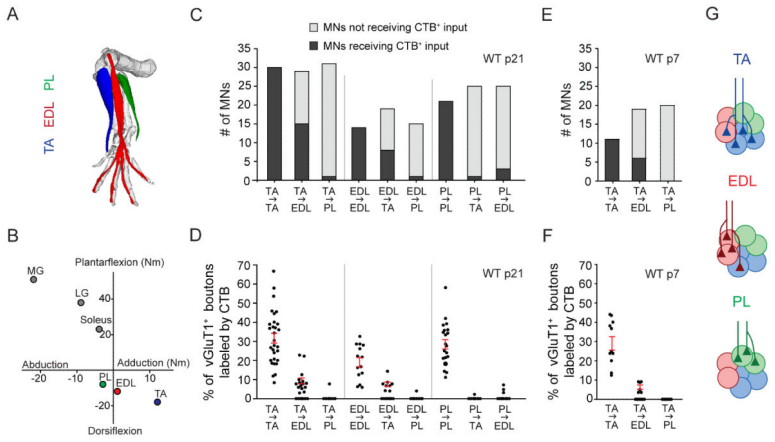

Figure 1. Patterns of Heteronymous Sensory-Motor Connections in the Anterolateral Crural Synergy Group

(A) Schematic of anterolateral crural muscle anatomy. TA = tibialis anterior. EDL = extensor digitorum longus. PL = peroneus longus. Image generated using The Mouse Limb Anatomy Atlas (Delaurier et al., 2008).

(B) Lines of action of muscles in cat. Axes represent torques (in newton-meters) evoked by individual muscle nerve stimulation. Posterior crural muscles shown in grey. MG = medial gastrocnemius. LG = lateral gastrocnemius. Adapted from (Nichols, 1994).

(C) Number of self and synergist motor neurons innervated by sensory afferents from a given muscle in p21 wild-type mice (n = 14-30 MNs; 3-7 mice per pair).

(D) Density of sensory synaptic connections with self and synergist motor neurons in p21 wild-type mice. Each point represents one motor neuron (n as in (C)). Red lines indicate mean ± SEM for motor neurons receiving input.

(E) Number of self and synergist motor neurons innervated by TA sensory afferents in p7 wild-type mice (n = 11-20 MNs; 2-3 mice per pair).

(F) Density of TA sensory synaptic connections with self and synergist motor neurons in p7 wild-type mice (n as in (E)).

(G) Schematic depicting organization of sensory-motor connectivity within the anterolateral crural synergy group.

All data reported as mean ± SEM. For related data, see also Figure S1.

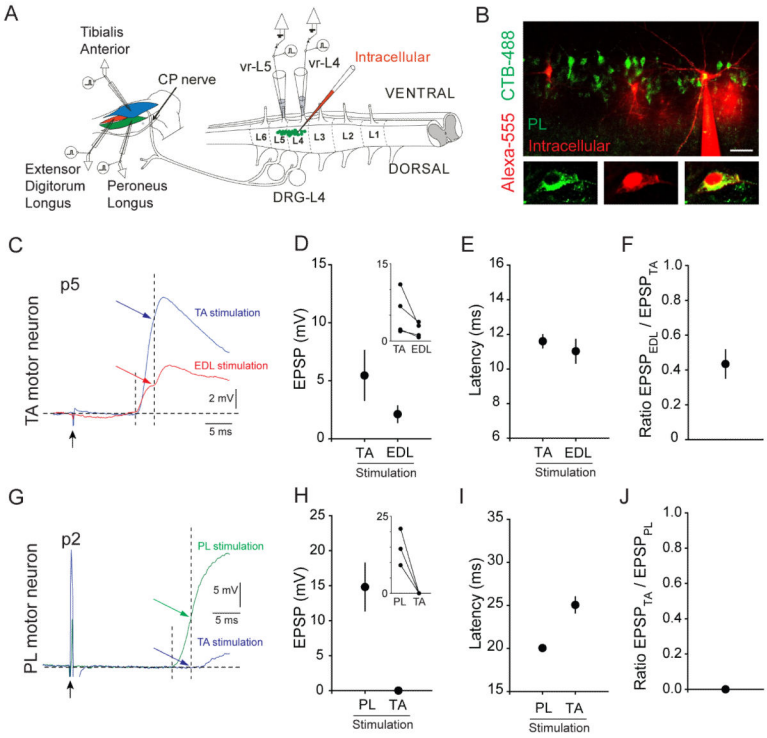

Figure 2. Functional Validation of Heteronymous Connections

(A) Schematic of lumbar spinal-hindlimb preparation. Stimulating electrodes were placed in TA, EDL, and PL muscles to activate proprioceptive fibers. Ventral roots were cut and placed into suction electrodes for either stimulation or recording. Motor neurons (green) were visually identified following muscle-specific labeling by CTB-488 and recorded intracellularly using whole-cell patch clamp.

(B) Image of PL motor neurons retrogradely labeled at p0 with CTB-488 and showing three cells filled with intracellular dye after whole-cell recording.

(C) Intracellularly recorded EPSPs in a single retrogradely labeled TA motor neuron upon stimulation of TA or EDL muscle. Traces averaged across 5 trials at 0.1 Hz. Black arrow indicates stimulus artifact. First dashed line indicates onset of EPSP response. Second dashed line indicates the maximum amplitude of the monosynaptic response, as determined at 3 ms after EPSP onset (Mears and Frank, 1997; Shneider et al., 2009).

(D) Average EPSP amplitudes induced in TA motor neurons upon TA or EDL muscle stimulation (n = 4 MNs). Inset represents corresponding relationship within each recorded motor neuron.

(E) Average latency of EPSP onset upon TA or EDL stimulation, as defined in relation to stimulus artifact.

(F) Average ratio of the EPSP amplitude induced in each TA motor neuron by EDL stimulation to the EPSP amplitude induced by TA stimulation.

(G) Intracellularly recorded EPSPs in a single retrogradely labeled PL motor neuron upon stimulation of PL or TA muscle. Single trials shown. The longer latency of response is due to the younger age at the time of recording. Conduction velocity increases with age due to a developmental increase in myelination (Li and Burke, 2002).

(H) Average EPSP amplitudes induced in PL motor neurons upon PL or TA muscle stimulation (n = 3 MNs).
(I) Average latency of EPSP onset upon PL or TA stimulation. Differences are significant at $p = 0.02$, indicating the lack of monosynaptic response from TA stimulation (Paired t-test).
(J) Average ratio of the EPSP amplitude induced in each PL motor neuron by TA stimulation to the EPSP amplitude induced by PL stimulation.
Scale bar represents 50 μm in (B). All data reported as mean ± SEM. For related data, see also Figure S2. For detailed methodology, see Supplemental Experimental Procedures.

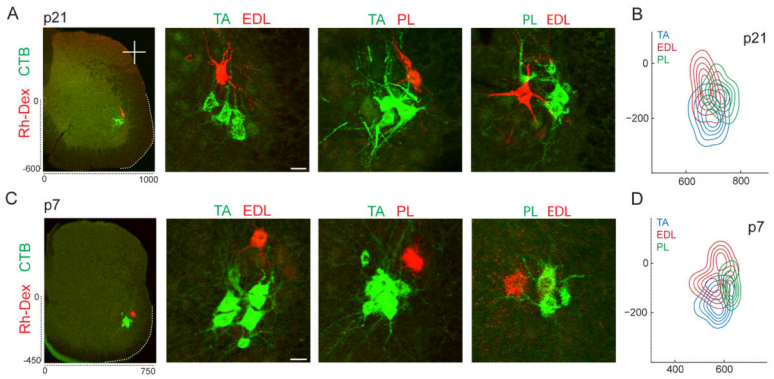

Figure 3. Spatial Organization within the Anterolateral Crural Synergy Group

(A and C) Organization of motor pool positions from L3-L4 in p21 (A) and p1-p7 (C) wild-type mice after CTB and Rh-Dex injection into specific muscles. Standard spinal cord dimensions shown in μm.

(B and D) Contour density plots showing the distribution of individual cell body positions at p21 (B) and p1-p7 (D). Position coordinates were determined as distance in micrometers with respect to the central canal and normalized to standard spinal cord dimensions. At both ages, X coordinates are significant between TA and PL, and EDL and PL at $p < 0.001$ (Student's t-test). At both ages, Y coordinates are significant between TA and EDL, and TA and PL at $p < 0.001$ (Student's t-test) (p21: TA: n = 99 MNs; 5 mice. EDL: n = 33 MNs; 4 mice. PL: n = 65 MNs; 4 mice. p1-p7: TA: n = 78 MNs; 5 mice. EDL: n = 32 MNs; 3 mice. PL: n = 30 MNs; 2 mice). Scale bars represent 30 μm in (A) and (C). For related data, see also Figure S3.

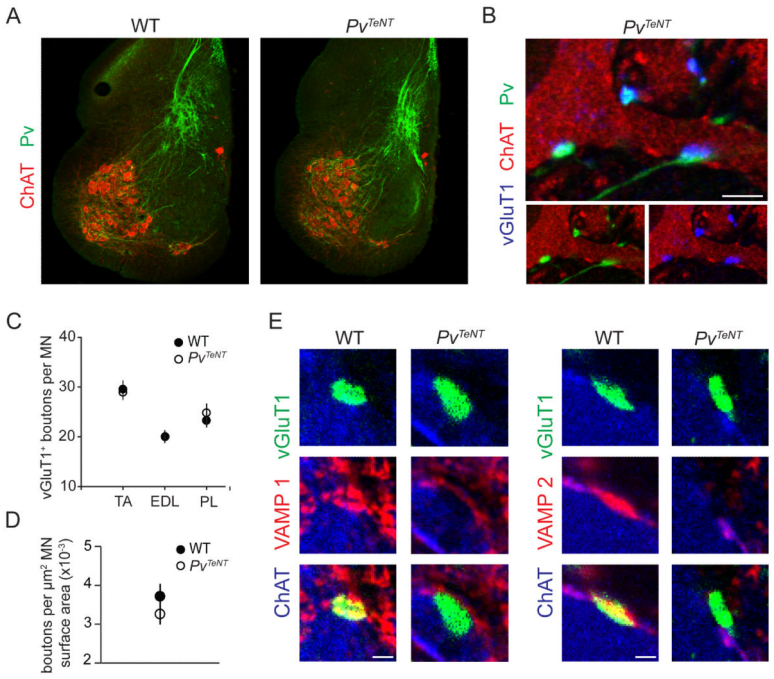

Figure 4. Sensory-Motor Synapses Maintained Following Tetanus Toxin Expression in Proprioceptors

(A) Axon trajectories of proprioceptor afferents in p8 wild-type and Pv^{TeNT} mice.

(B) Pv^{+}/$vGluT1^{+}$ boutons in contact with $ChAT^{+}$ motor neurons in p18 Pv^{TeNT} mice.

(C) Number of $vGluT1^{+}$ boutons on the soma and proximal ~100 µm dendrites in p21 wild-type and p18 Pv^{TeNT} mice (TA: WT n = 48 MNs, Pv^{TeNT} n = 40. EDL: WT n = 43, Pv^{TeNT} n = 25. PL: WT n = 52, Pv^{TeNT} n = 24).

(D) Density of $vGluT1^{+}$ boutons on motor neuron surface in p18 wild-type and Pv^{TeNT} mice (both WT and Pv^{TeNT}: n = 9 MNs; 3 mice).

(E) $vGluT1^{+}$ boutons in contact with $ChAT^{+}$ motor neurons no longer express VAMP 1 and VAMP 2 in p18 Pv^{TeNT} mice.

Scale bars represent 100 µm in (A), 5 µm in (B) and 2 µm in (E). All data reported as mean ± SEM. For related data, see also Figure S4.

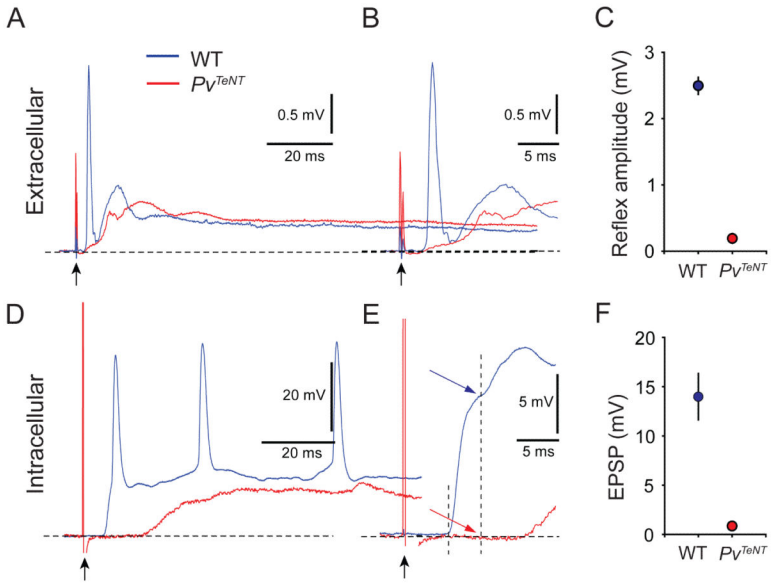

Figure 5. Tetanus Toxin Expression in Proprioceptors Blocks Sensory-Motor Transmission

(A and B) Extracellular recordings from ventral root L5 following dorsal root L5 stimulation in p8 wild-type and Pv^{TeNT} mice. Trace averaged across 5 trials at 0.1 Hz. Black arrow indicates stimulus artifact. Traces are shown in a time expanded scale in (B).

(C) Reflex amplitude is reduced by 92% in p8 Pv^{TeNT} mice. Differences are significant at $p < 0.001$ (Student's t-test, n = 3 mice).

(D and E) Intracellular recordings from L4 motor neurons following dorsal root L4 stimulation in p4 wild-type and Pv^{TeNT} mice. Single trials shown. Traces are shown in a time expanded scale in (E). First dashed line indicates onset of EPSP response. Second dashed line indicates the maximum amplitude of the monosynaptic response, as determined at 3 ms after EPSP onset.

(F) Monosynaptic EPSP amplitude is reduced by 96% in p4 Pv^{TeNT} mice. Differences are significant at $p < 0.001$ (Student's t-test; n = 4 MNs).

All data reported as mean ± SEM. For related data, see also Figure S5.

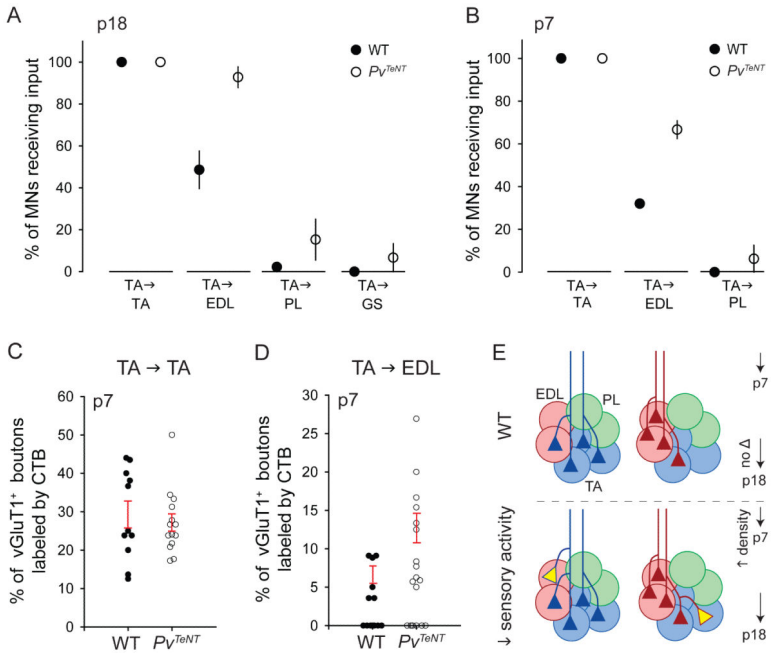

Figure 6. Increased Incidence of Heteronymous Connections Following Transmission Blockade

(A) Percentage of motor neurons contacted by TA sensory afferents in p21 WT and p18 Pv^{TeNT} mice (WT: data as in Figure 1C. Pv^{TeNT}: n = 3-5 mice). Difference in percentage of EDL motor neurons receiving TA input is significant at p = 0.003 (Student's t-test).

(B) Percentage of motor neurons contacted by TA sensory afferents in p7 WT and Pv^{TeNT}mice (WT: data as in Figure 1E. Pv^{TeNT}: 3-4 mice). Difference in EDL motor neurons receiving TA input is significant at p = 0.008 (Student's t-test).

(C) Density of TA sensory input to TA motor neurons in p7 wild-type and Pv^{TeNT}mice. Each point represents one motor neuron (WT: n = 11 MNs, as in Figure 1F. Pv^{TeNT}: n = 14 MNs). Red lines indicate mean ± SEM for motor neurons receiving TA input.

(D) Density of TA sensory input to EDL motor neurons in p7 wild-type and Pv^{TeNT} mice (WT: n = 19 MNs, as in Figure 1F. Pv^{TeNT}: n = 20 MNs). For EDL motor neurons contacted by TA sensory afferents, the density of contacts increases ~2-fold (p = 0.05; Student's t-test).

(E) In the absence of neurotransmission, sensory afferents contact a greater proportion of heteronymous motor neurons and initially contact each heteronymous neuron with increased density.

All data reported as mean ± SEM. For related data, see also Figure S6.

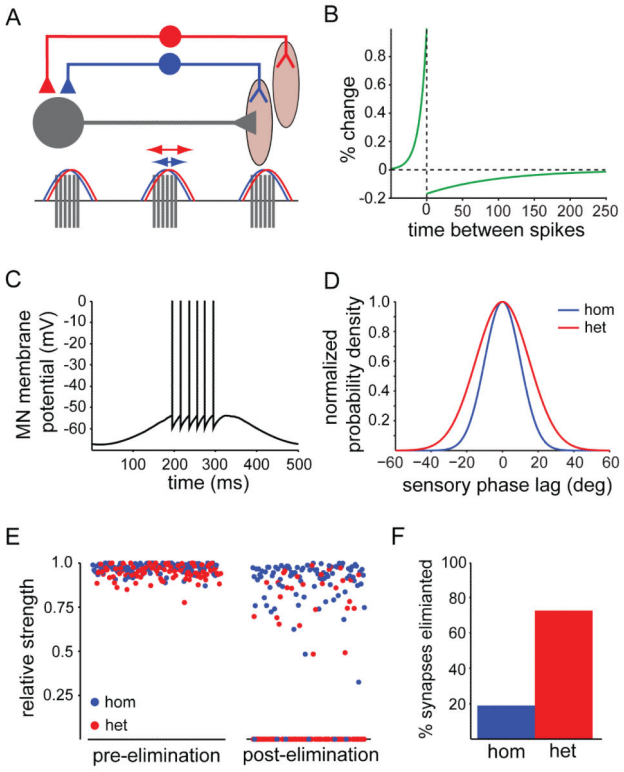

Figure 7. A Spike-Timing Model of Sensory-Motor Refinement

(A) Schematic of the spike-timing dependent plasticity model. A motor neuron (grey) receives sensory input from homonymous (blue) and heteronymous (red) sensory afferent populations. The strength of the sensory-motor synapses is subject to STDP, resulting in a dependence on the phase relationship between the firing patterns of the sensory afferent and the motor neuron.

(B) Long-tailed STDP model. The horizontal axis is the difference t_{pre}-t_{post} in ms between the pre- and postsynaptic spike times. The vertical axis is the change in synaptic strength relative to the maximal strength produced by a single spike pair.

(C) Simulated motor neuron spike train. The neuron fires a burst of ~6 spikes twice per second.

(D) Distribution of sensory afferent firing phases relative to the phase of the simulated motor neuron activity. On each cycle, homonymous and heteronymous afferent activity was phase shifted relative to the motor oscillation by a random amount chosen from a zero-mean Gaussian distribution with a standard deviation of 10 or 15 degrees, respectively (n = 100 each). The distributions shown have been normalized to a peak value of 1.

(E) Sensory-motor synapse strengths shortly after application of STDP model (left), and following application of model over 200 minutes of simulated muscle contraction (right). Synaptic strengths are reported in units of the maximum allowed synaptic strength (1 nS), and all synapses were set to a relative strength of 1.0 at the beginning of the simulation.

(F) Percentage of sensory-motor synapses refined during a representative application of the STDP model.